Optics and Lasers in Engineering 130 (2020) 106087

Contents lists available at ScienceDirect

Optics and Lasers in Engineering

journal homepage: www.elsevier.com/locate/optlaseng

Maximum smoothness consistent unwrapping of n-dimensional phase fields

Julio C. Estrada [a,*], Alonso Ramirez-Manzanares [a], Luis Concha [b], Jose L. Marroquin [a,*]

[a] *Centro de Investigacion en Matematicas, A.C., Guanajuato, Gto., Mexico*
[b] *Institute of Neurobiology, Universidad Nacional Autonoma de Mexico, Queretaro, Mexico*

ARTICLE INFO

Keywords:
Fringe analysis
Phase unwrapping
Magnetic resonance imaging
Phase measurement

ABSTRACT

The accurate recovery of an n-Dimensional field from observations that are wrapped into a particular interval (e.g., $[-\pi, \pi]$) is a problematic step in many applications, such as holography, interferometry, optical metrology, magnetic resonance imaging and analog-to-digital conversion in digital photography. While methods designed for this purpose abound (mainly in the 2-Dimensional case), most fail if the original unwrapped field contains abrupt changes that become aliased. In this paper we present Maximum Smoothness Consistent Unwrapping (MSCU), a novel and general method that overcomes said limitation. The method operates in two stages: in the first, a region without aliased changes which is as large as possible (which we call the consistent region) is found, and in the second, the unwrapped phase in the consistent region is propagated to the inconsistent areas to get the final result. MSCU has the following advantages: it is well founded theoretically, which allows the assessment of the reliability of its results; it is directly applicable to fields in any number of dimensions and when the signal is wrapped module any real number P; it has no free parameters to adjust; and it is computationally efficient and easy to implement. We present a formal derivation of the method and illustrations of its performance, both in synthetic fields –where we compare it with that of other state-of-the-art methods– and in real data (2-D data from optical speckle interferometry and 3-D data from magnetic susceptibility images obtained by magnetic resonance acquisitions). In this paper we focus on phase unwrapping applications, but the presented method may be directly applied to the case of other wrapping intervals as well, as for instance in High Dynamic Range image processing.

1. Introduction

Recovering a signal from data that has been wrapped into a given interval is a problem that is relevant in several areas, such as optical interferometry [1,2] and radar interferometry [3,4]. In Magnetic Resonance Imaging (MRI), phase images show modulations resulting from magnetic susceptibility which are the consequence of biologically-relevant tissue characteristics that change the local resonance frequency as a function of the geometry of the object [5]. In digital photography the unwrapping problem can be seen in High Dynamic Range (HDR) images, as camera sensors self-reset the pixel voltage on saturation, wrapping image intensity into a given voltage interval [6,7].

A solution for the unwrapping problem that is *compatible* with the data is found by adding to the wrapped phase at each point an integer multiple of the wrapping interval (2π for phase fields), and many methods have been proposed to find it [3,8–11]. The majority of previous methods are based on the estimation of the derivatives (gradient or Laplacian) of the unknown unwrapped field using the given wrapped data. Once these derivatives are estimated, the corresponding fields are integrated to obtain the desired solution, either in the image domain following appropriate paths or in the frequency domain [11]. The difficulties with this type of approaches arise when the original unwrapped field contains abrupt changes (jumps or barriers), whose magnitude is greater than half the wrapping interval (i.e., greater than π radians for phase fields), in which case the derivatives of the wrapped data will not be good estimates of the true derivatives. When this occurs we say that the original field contains *barriers*, which causes the wrapped field to be *inconsistent* in the sense that the integration of the derivative fields may produce different results depending on the integration path.

To deal with this problem, some methods choose integration paths in a way that regions where the wrapped field is likely to be consistent are unwrapped first, so that when inconsistent regions are unwrapped there is sufficient correct information around them to prevent the propagation of errors [10,12–14]. However, the criteria used for path selection is based on properties of the derivatives themselves, and these properties are not necessarily related to the barriers that may be present and generate inconsistencies, because the wrapping process aliases the field so that even across barriers the derivatives of the wrapped data may be arbitrarily small (see example in the Experiments section). Examples of these methods include branch cuts [13], following level curves of the wrapped field [15] or unwrapping regions where the wrapped differences are small [14]. Although all of these methods work well in many

* Corresponding author.
E-mail addresses: julio@cimat.mx, jlm@cimat.mx (J.C. Estrada), julio@cimat.mx (J.L. Marroquin).

https://doi.org/10.1016/j.optlaseng.2020.106087
Received 9 December 2019; Received in revised form 5 February 2020; Accepted 2 March 2020
Available online 14 March 2020
0143-8166/

cases, they may fail unpredictably in others and there is no way (other than a subjective visual inspection) to determine if the results for a given data set are correct.

In a different approach, the unwrapped solution is found by minimizing a cost function [16–18], so that the reconstructed unwrapped field is maximally smooth. The problem here is that the resulting field is, in general, not compatible with the data, since this process reduces the dynamic range of the estimated unwrapped signal [17,18]. Besides, these algorithms use some free parameters with no principled way to determine their value, so there remains a degree of arbitrariness in the solution.

The 3–dimensional unwrapping problem is important in applications such as radar interferometry (InSAR) time series, and MR medical images. Some unwrapping methods that have been proposed for this case are extensions of quality-guided strategies [19,20] and have, therefore, the same limitations. Another approach is used in [21]. There, derivatives of the wrapped phase are corrected by eliminating spurious peaks. These corrected derivatives are then used to adjust an analytic function (a linear combination of complex exponentials) using a least squares approach; from this fitted function a compatible estimate for the unwrapped phase is constructed. Similarly to quality-guided strategies, the problem is that if the original wrapped field contains barriers, the phase derivatives will be aliased by the wrapping process and the adjusted analytic function will not be close to the true value. A different approach is provided in [22], based on the strong assumption that the phase difference in one dimension is smooth enough such that a 1–dimensional unwrapping can be performed independently of the other two dimensions; however, it is common that noise affects the wrapped signal, so, in general, that assumption is not met.

We propose a method based on a solid mathematical foundation that produces a field compatible with the data, without free parameters, that is directly applicable to n–dimensional fields, and that permits the determination of the correctness of the results it produces. In the following sections, we describe the method and show tests and results.

2. Methods

Although most instances of the unwrapping problem occur for phase fields which are wrapped into $[-\pi, \pi]$ radians, here we consider the general case where the signal is wrapped into any real interval [*a, b*], where units depends on the particular application. In precise terms, we can describe the unwrapping problem of n-dimensional module signals as follows: consider an n–dimensional lattice L of voxels and an unknown field h on L. What is available to us is a field h_w which corresponds to h wrapped into the interval [*a, b*]. Given this, we want to recover the unwrapped field h. The method presented here requires that the input data are wrapped into [0,1]; a normalized unit-less range. To obtain this, one may transform the data h_w into a new field w using:

$$w(u) = \frac{h_w(u) - a}{b - a}$$

for every voxel $u \in L$. For phase fields we have that $a = -\pi$ and $b = \pi$, then $w(u)$ is defined as:

$$w(u) = \frac{h_w(u) + \pi}{2\pi}. \tag{1}$$

Once one finds from w an estimate $\hat{g}$ for the unwrapped transformed field, one can recover an estimate $\hat{h}$ for the original field h using the inverse transformation, which for phase fields is:

$$\hat{h}(u) = 2\pi\hat{g}(u) - \pi. \tag{2}$$

In what follows, we consider therefore the following problem: given the normalized wrapped field $w(u) \in [0, 1]$, for $u \in L$, the task is to estimate a field $\hat{g}$ given by:

$$\hat{g}(u) = w(u) + z(u), \tag{3}$$

where z must be a field of integers, so that $\hat{g}$ is compatible with w.

The difficulty here is that this problem does not have a unique solution since it is mathematically ill-posed [9,23,24]. To solve it, one must make some assumptions about g. What is usually done is to assume that g is as smooth as possible. The strategy used by most used algorithms in practice [8], which we call the Path Unwrapping Algorithm (PUA), consists in following a set of paths of consecutive points $p_1, p_2, \dots, p_N$ in L such that $\|p_k - p_{k-1}\| = 1$ for $k = 1, 2, \dots, N$. All these paths start from a seed point s_0, so we set $\hat{g}(p_1) = w(p_1) = w(s_0)$ and find for each consecutive point the unwrapping integer $z(p_k)$ that makes the resulting field as smooth as possible along this path. This results in the following update rule:

$$\hat{g}(p_k) = w(p_k) + R[\hat{g}(p_{k-1}) - w(p_k)], \tag{4}$$

where $R[\,\cdot\,]$ is the signed rounding operator: $R[x] = sign(x) \cdot \lfloor |x| + 0.5 \rfloor$, where $\lfloor y \rfloor$ takes the integer part of the positive number y. Note that $R[x]$ finds the integer that is closest to $|x|$ with the appropriate sign; this implies that

$$|R(x) - x| < 0.5. \tag{5}$$

In general, for a given field w and a region Ω the result of the application of (4) from a given seed point s_0 to a final point $p_N \in R$ will depend on the path from s_0 to P_N. If this is not the case and the result is path-independent (i.e., it is equal for all seed points and all final points), we say that w is *consistent* in Ω. If this happens and one now subtracts $\hat{g}(p_{k-1})$ from both sides of Eq. (4) and takes absolute values one obtains from (5):

$$|\hat{g}(p_k) - \hat{g}(p_{k-1})| = |-(\hat{g}(p_{k-1}) - w(p_k)) + R[\hat{g}(p_{k-1}) - w(p_k)]| < 0.5.$$

So that, along any path in a *consistent* region Ω

$$|\hat{g}(p_k) - \hat{g}(p_{k-1})| < 0.5. \tag{6}$$

An important consequence of this is the following:

Proposition 1. *If for all pairs r, s of neighboring points in L i.e., points with* $\|r - s\| = 1$, *the original field g satisfies* $|g(r) - g(s)| < 0.5$ *the results of applying the PUA will not depend on the chosen paths. In this case, we say that the field g is barrier free and the field w is consistent (the proof is presented in the appendix).*

The concept of barriers, that is, pairs of neighboring points *r, s* with $|g(r) - g(s)| \geq 0.5$, is similar to the one used in branch cut methods [8]. If the field g contains barriers, and these barriers are open, in the sense that there are paths between r and s that do not cross any barriers while other paths cross at least one, the field w will be inconsistent and the results of the PUA will not be path-independent, since any path that goes through a barrier will give different results from paths that go around it. As a result of this, the field $\hat{g}$ produced by the PUA will contain spurious barriers that in general will not coincide with the actual barriers in g. In fact, a single pair of barrier voxels in g may cause the PUA to propagate the error and produce incorrect unwrapping results in large regions of L. Note that if g contains open barriers, the desired $\hat{g}$ should also contain them and they should be as close as possible to those of g.

In real scenarios, barriers may be introduced in g not only by discontinuities that may be present in the actual signal, but also by noise in the sensing process, so that dealing with inconsistent wrapped data is an important problem.

The general idea of the method proposed here, which we call Maximum Smoothness Consistent Unwrapping (MSCU) is to find, in a first stage, a set $C \subseteq L$ of voxels which is as large as possible and where w is consistent, so that the PUA produces results which are independent of the path chosen. Once this is done, in a second stage one fills the complement of C (the zone with inconsistencies) with a technique that we call dilation unwrapping, which produces as an end result a field $\hat{g}$ that is compatible with w and whose barriers are as close as possible to those of g.

To derive the method, first one needs to characterize the region C where w is consistent. As explained above, this region is characterized

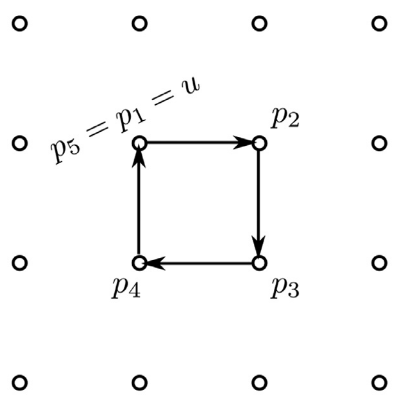

Fig. 1. An scheme of the path that follows the inconsistency condition in (7).

by the fact that for *all* closed paths that lie in C i.e., paths with $p_1 = p_N$ for all possible $p_1 \in C$ and N, one finds $\hat{g}(p_N) = \hat{g}(p_1)$ after applying (4). This condition however is prohibitively expensive to test. In the 2-dimensional case a simpler condition is to test only closed paths with 4 points that form a square one-pixel wide with one corner at the pixel u [8]. This condition is equivalent to the following:

$$\sum_{k=1}^{4} R[w(p_k) - w(p_{k+1})] = 0 \tag{7}$$

where $p_5 = p_1 = u$ as illustrated in Fig. 1. In the case of 3 or more dimensions this condition should be checked for all possible planes obtained by taking different pairs of dimensions at a time; in 3 dimensions for example, for the $x-y$, $x-z$ and $y-z$ planes.

If (7) is not met, we say that there is a local inconsistency in the 4 neighboring coplanar voxels used to compute (7).

Even if locally inconsistent voxels are removed, however, the region may remain inconsistent because local inconsistencies are generated only at the end points of open barriers, and the rest of the barriers may be aliased by the wrapping operator and will remain hidden and impossible to detect. The proposed strategy then is to erode the consistent region until the complete barriers - whose location is unknown - are covered. To do this, one needs a computationally efficient way to determine if w is consistent in any path-connected region. This is obtained by the following:

Proposition 2. *The wrapped field w is consistent in a path-connected region C if and only if the field $\hat{g}$ - obtained by applying the PUA in this region from a seed point $s_0 \in C$ and following paths that lie in C - is barrier-free (the proof is presented in the appendix).*

The idea of the method then, is to start with a candidate consistent region which is equal to the complete lattice excluding the pixels where local inconsistencies have been detected and apply the PUA in this region. One can then test for the consistency of this region using Proposition 2 and if this test fails, incrementally erode it and repeat the unwrapping until the barrier-free condition of the unwrapped field is satisfied and one can proceed to the next stage. The first stage of the process therefore is:

Stage 1

1. Find the set of voxels with local inconsistencies and set C as its complement, that is, the voxels with no local inconsistencies. Use (7) to find the local inconsistencies.
2. Apply the PUA in C to find a field $\hat{g}(u), u \in C$.
3. Test if w in C is consistent by verifying if $\hat{g}$ is barrier-free in C.
4. If w is not consistent, obtain a new region C by applying to it an incremental erosion operator E (see [25]), i.e., set $C := E[C]$, and repeat from step 2
5. End.

When this process is completed, we know that the unwrapping is consistent in the resulting region C, so that the local and global inconsistencies are confined to the set C^c (the complement of the resulting C).

Now we describe these steps in more detail: To find a field $\hat{g}$ in step 2, we propose the following simple algorithm which unwraps w in a path-connected region C from a seed point $s_0 \in C$. It uses a queue Q of pixels and an auxiliary field m which indicates which pixels $\hat{f}$ have already been computed. Let $\mathcal{N}(r) = \{s : ||r-s|| = 1\}$; the detailed algorithm for step 2 is as follows:

{

1. Set $Q = \emptyset$ (the empty queue);
2. Set $m(r) = 0$ and $\hat{g}(r) = 0$ for all $r \in L$;
3. Set $m(s_0) = 1$; $\hat{g}(s_0) = w(s_0)$; Push s_0 into Q
4. While $Q \neq \emptyset$ do:
   (a) Get r from Q;
   (b) For all voxels $s \in \mathcal{N}(r)$ such that $s \in C$ and $m(s) = 0$
      (1) Set $\hat{g}(s) = w(s) + R[\hat{g}(r) - w(s)]$;
      (2) Set $m(s) = 1$;
      (3) Push s into Q

}

Note that in this algorithm many paths are considered at the same time, all with the same starting point s_0, and with their current end-points stored in Q, which are followed until all points in $\hat{C}$ are correctly unwrapped.

For step 3, the test to determine if w is consistent in C is obtained directly from Proposition 2:

$$\max_{\langle r,s\rangle \in C} |\hat{g}(r) - \hat{g}(s)| < 0.5, \tag{8}$$

where $\langle r, s\rangle$ denotes all pairs of neighboring points. The incremental erosion operator E that is used in step 4 is the morphological erosion [25] using as structural element an $n-$dimensional sphere with unit radius:

$$E[C] = \{r \in C : \mathcal{N}_r \subset C\}.$$

Once these steps are completed and the test (8) is passed, one proceeds to the second stage which consists in progressively dilating the region C (see [25]), extending the field $\hat{g}(u), u \in C$ using Eq. (4) at each step, so that the solution in C is propagated until the complete image is unwrapped. To do this, if there is more than one voxel in C from which the unwrapped field may be propagated to a neighboring voxel $r \in C^c$, we select the one that maximizes the smoothness i.e., the one that minimizes the absolute difference between the new unwrapped value and that of the corresponding neighbour. The detailed algorithm for this stage is as follows:

Stage 2. Dilation and Propagation

1. Find the set B of boundary pixels of C^c:

   $$B = \{r \in C^c : \mathcal{N}_r \bigcap C \neq \emptyset\}$$

2. For each pixel $r \in B$ do:
   (a) Find the pixel $u^* \in \mathcal{N}_r \bigcap C$ such that $|w(r) + R[\hat{g}(u^*) - w(r)] - \hat{g}(u^*)|$ is as small as possible.
   (b) Set $\hat{g}(r) = w(r) + R[\hat{g}(u^*) - w(r)]$
3. Set $C := C \bigcup B$
4. if $C^c \neq \emptyset$ go to step 1.
5. End.

In this algorithm we use $\mathcal{N}_r$ as the $n-$dimensional sphere with unit radius with center r.

Note that by construction the algorithm will locate the barriers in $\hat{g}$ approximately at the medial axes (morphological skeletons) of the inconsistent connected regions that constitute C^c so that, although the location of the original barriers of g cannot be uniquely determined from w, the only information being that their end points are located at the

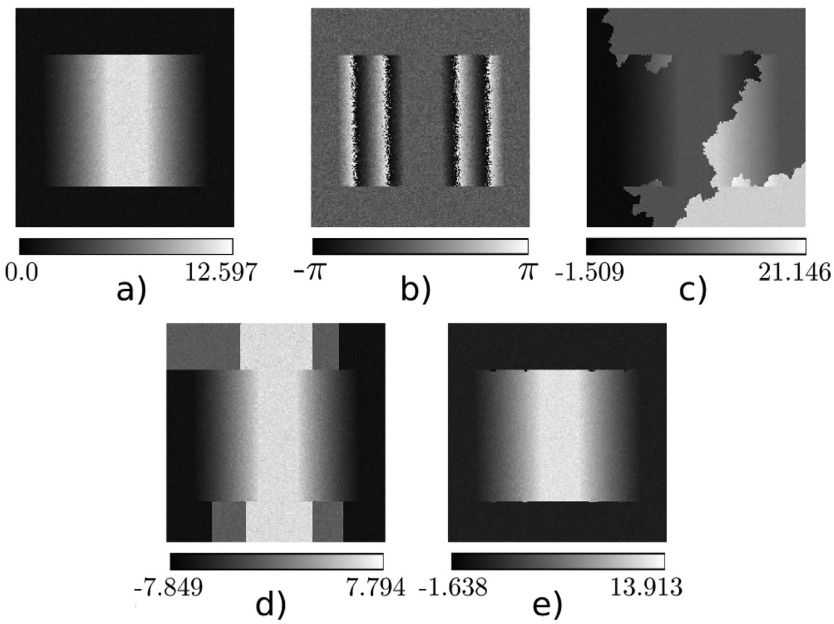

Fig. 2. An illustrative synthetic example with dimensions 256 × 256 pixels. (a) Original unwrapped field. (b) Wrapped data. (c) Unwrapped result using the algorithm in [14]. (d) Unwrapped result using the algorithm in [13]. (e) Unwrapped result using the method presented here. The units here are radians.

local inconsistencies of w, the proposed method will find the shortest possible barriers in the compatible field $\hat{g}$ which also end at the local inconsistencies.

In summary, the complete algorithm for the MSCU method is as follows:

Complete algorithm

1. Transform the given wrapped data into the interval [0,1] using Eq. (1) ;
2. Run **Stage 1** of the process to find the largest possible region C where the transformed wrapped phase w is consistent;
3. Using **Stage 2**, progressively dilate C propagating the solution in C^c until the complete unwrapped field $\hat{g}$ is computed;
4. Find the final estimated unwrapped field $\hat{h}$ using Eq. (2);

Note that if the original unwrapped field is barrier-free, the region C found in Stage 1 will coincide with the complete lattice, so that neither erosion nor dilation will be necessary and MSCU will perform a perfect reconstruction in one step. It should be noted that in this case any one of the traditional path following algorithms will exhibit an equivalent performance, since the propagated solution found by the PUA algorithm will not depend on the path. However, if there are barriers present in the original field, traditional path following algorithms will fail and spurious discontinuities will appear in the solution at places that depend on the particular unwrapping path, whereas MSCU will produce the correct solution.

3. Experiments

We designed an illustrative and simple synthetic example that contains barriers along open curves, a scenario that proves difficult for commonly used unwrapping methods, and we used it to study the performance of MSCU and other published methods. In particular, we compare the performance of MSCU with two of the most widely used unwrapping methods for which the authors provide the corresponding codes, so that implementation issues are avoided. This example field appears in panel (a) of Fig. 2 and consists of two ramps of opposite slope at the center of the image which rise from a constant plane at height zero to a top plane of an arbitrary height 4.015π radians. This was done so that the height differences across the barriers appear aliased in the wrapped field. The image was then corrupted by additive white Gaussian noise with 0 mean and variance equal to 0.12π radians. In panel (b) the corresponding wrapped image is presented. Note that the barriers produced by the height differences between the top and the bottom planes in (a) appear aliased in the wrapped field. This example was contrived to highlight the weak points of existing algorithms, but the situation it portrays often occurs in practice, specially in noisy and/or high gradient wrapped fields. Panels (c) through (f) present the unwrapped phase recovered using different methods.

Panel 2(c) shows the result obtained with the algorithm in [14] in which the fields of horizontal and vertical first order wrapped differences are integrated following a path guided by the magnitude of the second order wrapped differences, so that the unwrapping is performed first along regions with the least possible variation. The problem is that if the barriers in the original field are aliased in the wrapped field, as in this example, the first and second order differences across them may be small, so that the unwrapping paths may cross the barriers at early stages and produce erroneous results as the one shown here. The required time for this method is 26.6 microseconds in a computer with an Intel(R) Core(TM) i5-6300U-2.40 GHz (the same computer was used to measure the time for all the following 2D experiments).

Panel 2(e) shows the result obtained using [13], which is one of the most recent branch-cut algorithms published. In this approach local inconsistencies are detected (see Fig. 3(a)) and connected with a branch-cut that cannot be crossed by the unwrapping paths. However, finding the right connections between local inconsistencies is not an easy task because there may be many different possible connection combinations. In [13] they are connected based on their proximity, but in this case, this fails to establish the appropriate branch cuts along the true barriers. In particular, inconsistencies labeled as 1 and 2 in Fig. 3(a) and those labeled as 3 and 4 are connected, but not those labeled as 2 and 3 as it should be. As a result, although the ramps and top plane are correctly unwrapped, the method introduces spurious jumps in the constant plane at height zero, so that the complete field is not correctly unwrapped. The required time for this method is 12.6 microseconds.

Finally, panel 2(f) presents the result obtained with MSCU, the method presented here. In this case the region without local inconsistencies (see Fig. 3(a)) is eroded until the test (8) is satisfied (see Figs. 3 (b) and (c)), and then the dilation and propagation procedure is applied to obtain the final result which as one can see is practically indistinguishable from the ground truth, except for an additive constant and small errors close to the boundaries. The required time for our proposal is 11.66 microseconds.

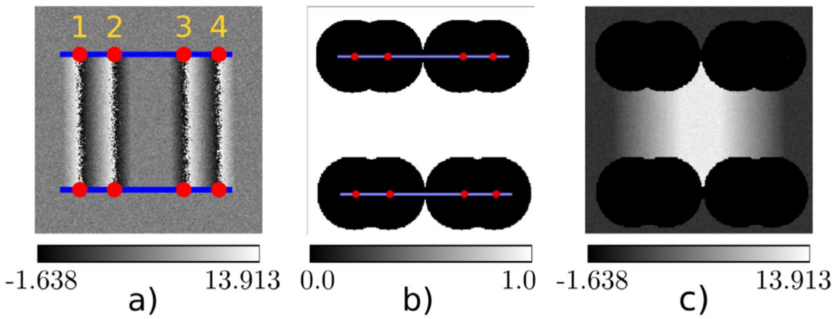

Fig. 3. Details of the operation of MSCU unwrapping in the example of Fig. 2. (a) Detected local inconsistencies (red dots). (b) The eroded consistent region appears in white. (c) Unwrapped phase in the consistent region. The result in Fig. 2(f) is obtained after the dilation and propagation procedure described in the text. The units here are radians. (For interpretation of the references to colour in this figure legend, the reader is referred to the web version of this article.)

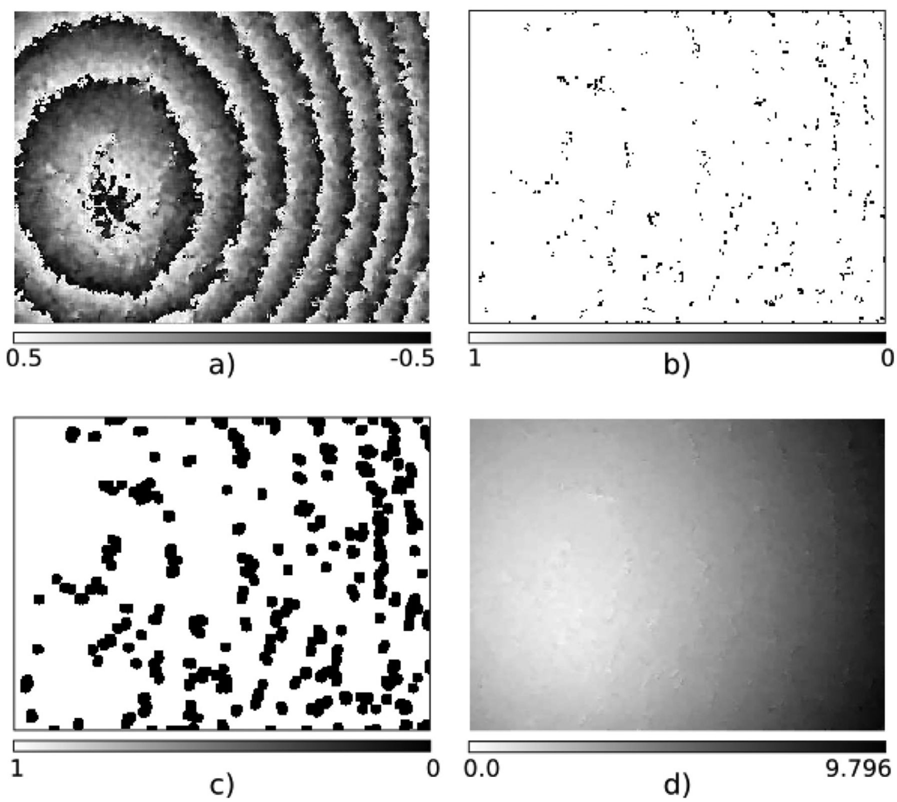

Fig. 4. Experimental wrapped phase from speckle interferometry. The size of the image is 482 × 641 pixels. (a) Wrapped phase, (b) Local inconsistencies, (c) Consistent region after erosion, and (d) Final result. Dynamic range of phase images $\times 2\pi$ represent radians.

In the next example, we unwrap the phase that is obtained from an experiment that uses the electronic speckle interferometry technique (ESPI). In Fig. 4(a) we show the wrapped phase, in Fig. 4(b) we show the local inconsistencies which are introduced by speckle noise; in Fig. 4(c) the consistent region that results from the erosion process and in Fig. 4(d), the final result produced by MSCU. The required time for our proposal is 448.1 microseconds. It is important to note that in this example, simply masking out the local inconsistencies and applying the PUA algorithm will not give correct results, which indicates that configurations with aliased open barriers such as the ones presented in the synthetic example above are also present in this case.

The next experiment presents the application of our methodology to the problem of unwrapping of 3D MR magnetic susceptibility weighted imaging (SWI-MR) phase data. This type of images have several clinical applications; for example, it is known that magnetic susceptibility is altered by the accumulation of iron, and has been demonstrated to be abnormal in patients with certain neurodegenerative diseases [26,27]. Susceptibility-weighted imaging is also used in the clinic to image vessels, hemorrhages, and calcium deposits in the brain, and has been extended for quantification purposes as quantitative susceptibility mapping (QSM) [28]. However, an imperfect magnetic field induces further phase changes and high phase gradients that contaminate the inhomogeneities caused by the phenomenon being studied [29], and is the major hurdle preventing accurate interpretation of these imaging methods. To account for these effects without introducing additional artifacts it is important to have an accurate, compatible and truly 3D unwrapping of the field. In the experiment presented here, written informed consent was obtained from the volunteer participating in this study. Images were acquired in one healthy adult female volunteer using a Philips Achieva TX 3.0 T scanner and a 32-element head coil. SWI-MR was acquired using an axial 3-dimensional gradient echo sequence (TR=19.9 ms; TE=28 ms; α=10°; FOV=220 × 180.5 × 99 mm^3, left-right phase-encoding direction). Acceleration using SENSE [30] was implemented in the phase (× 2.5) and slice (× 2) dimensions. The high–resolution volume consists of 330 slices with 512 × 512 voxels each. 3D Phase unwrapping was applied to the wrapped-phase volume.

A detailed 3D view of the results on the volume are shown in Fig. 5, which shows axial, coronal and sagittal slices of the results around the middle of the brain with center in the coordinates (256,261,170). We present the input and output fields in false color map, as this representation enhances the conspicuity of protuberances in the unwrapped field that indicate a change in the anatomy of the subject. First row

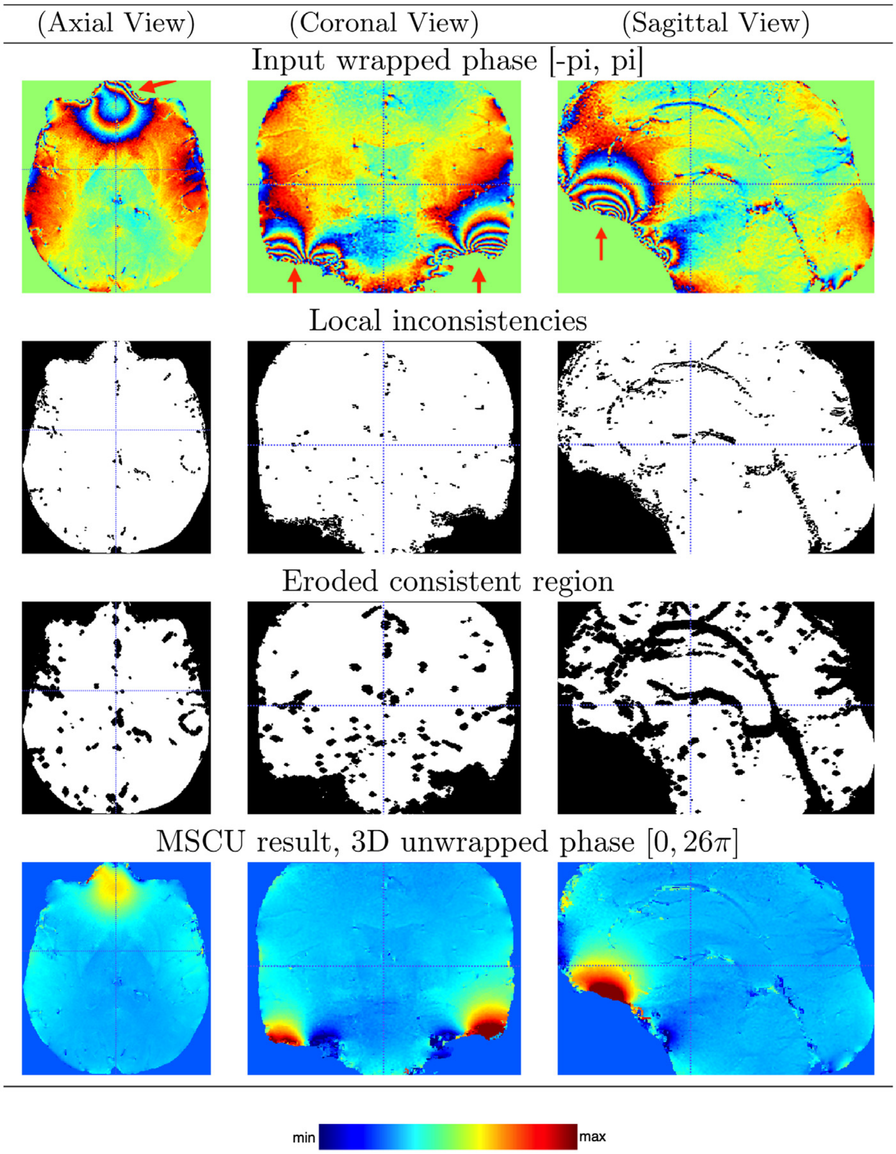

Fig. 5. Multi-slice visualization (with the columns corresponding to the axial, coronal and sagittal views) for the SWI-MRI phase data. We show in the first row the input wrapped data (dynamic range: $[-\pi, \pi]$); in the second row the map of local inconsistencies; in the third row the eroded consistent region (in white) and in the fourth row the unwrapped field estimated by MSCU (dynamic range: $[0, 26\pi]$).

shows the input (wrapped) data, the map of the local inconsistencies is shown in second row. The eroded consistent regions are shown in the third row. Finally the unwrapped phase given by our method is shown in the bottom of the Figure. Note the conspicuous phase gradients seen in the input wrapped phase maps near air-tissue interfaces, such as the frontal pole, and the basal aspect of the temporal lobes (red arrows), that are correctly unwrapped and appear smooth in the MSCU results in the 4–th row. The 3-D ANSI-C implementation on an Intel Core i7-4771 CPU running at 3.5 GHz took around 19 s to process the complete volume.

4. Discussion and conclusions.

We have presented an unwrapping algorithm for fields on any number of dimensions. For most applications, 2 or 3 dimensions are sufficient, but the method presented here is directly applicable to higher dimensions as well. The method is simple to implement and computationally efficient, note that the required time in our experiments is smaller with respect to the required time by the previously proposed methods we compare with. The MSCU method presented here has the following features:

1. It permits the estimation of a region C where the given unwrapped phase w is consistent.
2. Once this is found, it finds an estimated unwrapped field that is compatible with w everywhere and that in C is as smooth as possible.
3. In the complementary region C^c it finds a field that is as close as possible to a smooth extension of f in C. Note that in this region f may be neither smooth (it may contain discontinuities) nor consistent.
4. The procedure is simple to implement and computationally efficient (about 19 seconds in a full 3-D implementation on a 3.5 GHz processor for the 3D volume in Fig. 5, i.e. approximately 0.06 seconds for each 512×512 slice).
5. Although this paper is focused on phase fields wrapped into the interval $[-\pi, \pi]$ the method is directly applicable to any other wrapping interval.

MSCU finds a solution to the ill-posed unwrapping problem that is maximally smooth and that is consistent in a region which is as large as possible. The method has no free parameters to adjust since it uses a data–dependent rigorous criterion to determine the smallest number k^* of erosion operations, applied to the region without local inconsistencies, that are needed to define C.

Finally, note that our method also may provide a data–dependent measure for the reliability of a solution, namely the ratio ρ of the number of voxels in the consistent region C obtained after the erosion operation to the total number of voxels in the region of interest: if ρ is close to zero, it means that the original field contains discontinuities that are too extensive, so that C is too small for the smooth extension of f to be a good approximation to the solution, whereas values of ρ close to 1 indicate a highly reliable solution. Thus, ρ is defined as:

$$\rho = \frac{D\{C\}}{D\{\hat{g}\}},$$

where $D\{C\}$ and $D\{\hat{g}\}$ are the number of voxels/pixels in region C and image $\hat{g}$, respectively. For example, ρ is equal to 0.4826, 0.8135, and 0.87 for experiments in Figs. 3, and–5, respectively.

Contributions

J.C.E. and J.L.M. contributed in concept formulation and drafted the original version of the manuscript. A.R.M. and L.C. were involved in medical data acquisition, analysis and validation. All authors reviewing and approved the final version of the manuscript.

Declaration of Competing Interest

The authors declare no competing interests.

In summary, we presented a novel method with a robust theoretical foundation that is free of user-parameters and is able to correctly unwrap data with abrupt changes. At last but not least, this method can be applied on data with an arbitrary number of dimensions and it is computationally efficient.

Acknowledgements

The authors thank Dr. Erick Pasaye and staff at the National Laboratory for MRI (which has received funding from Conacyt 232673, 251216, 280283 and 293394) for help during MRI data acquisition. LC is partially funded by Conacyt FC1782.

Appendix A

In this appendix we present the proofs of the Propositions 1 and 2 presented in the text.

Proposition 1. *If for all pairs r, s of neighboring points in L, i.e., points with* $\|r - s\| = 1$, *the original field g satisfies* $|g(r) - g(s)| < 0.5$ *the results of applying the PUA will not depend on the chosen paths.*

To see this, note that if $\hat{g}(p_{k-1}) = g(p_{k-1})$ *then* $\hat{g}(p_k) = g(p_k)$ *because since g is compatible with w and* $R[g(p_{k-1}) - g(p_k)] < 0.5$, *both* $\hat{g}(p_k)$ *and* $g(p_k)$ *are obtained by adding to* $w(p_k)$ *the integer that makes* $|g(p_{k-1}) - g(p_k)|$ *as small as possible. Assuming* $g(s_0) = w(s_0)$ *we get by induction that* $\hat{g}(p_N) = g(p_N)$ *independently of the intermediate points of the path.*

Proposition 2. *The wrapped field w is consistent in a path-connected region C if and only if the field* $\hat{g}$ *- obtained by applying the PUA in this region from a seed point* $s_0 \in C$ *and following paths that lie in C - is barrier-free.*

To prove it, we note the fact that if $\hat{g}$ *is barrier-free then w is consistent; this is established using the arguments given in the proof of Proposition 1. Conversely, to show that if w is consistent then* $\hat{g}$ *must be barrier-free, consider any two neighboring points r, s* $\in C$ *and the path used to get from* s_0 *to r. Since we are assuming that w is consistent we may add the point s at the end of this path to get* $\hat{g}(s)$, *and from (6)*

Supplementary material

Supplementary material associated with this article can be found, in the online version, at 10.1016/j.optlaseng.2020.106087.

References

[1] Hariharan P. Optical Interferometry. 2nd. Academic Press; 2003. ISBN 9780123116307

[2] Schnars U, Falldorf C, Watson J, Jüptner W. Digital Holography and Wavefront Sensing: Principles, Techniques and Applications. Springer Berlin Heidelberg; 2014. ISBN 9783662446935, https://books.google.com.mx/books?id=Nu6PBAAAQBAJ

[3] Goldstein RM, Zebker HA, Werner CL. Satellite radar interferometry: Two-dimensional phase unwrapping. Radio Science 1988;23(4):713–20. doi:10.1029/RS023i004p00713. http://doi.wiley.com/10.1029/RS023i004p00713

[4] Rosen P, Hensley S, Joughin I, Li F, Madsen S, Rodriguez E, et al. Synthetic aperture radar interferometry. Proceedings of the IEEE 2000;88(3):333–82. doi:10.1109/5.838084. http://ieeexplore.ieee.org/document/838084/

[5] Haacke EM, Brown RW, Thompson MR, Venkatesan R, et al. Magnetic resonance imaging: physical principles and sequence design, 82. Wiley-Liss New York:; 1999.

[6] Lukac R. Computational Photography: Methods and Applications. CRC Press; 2017. ISBN 9781439817506, https://books.google.com.mx/books?id=rGWxB7rkJl8C

[7] Zhao H, Shi B, Fernandez-Cull C, Yeung S-K, Raskar R. Unbounded High Dynamic Range Photography Using a Modulo Camera. In: 2015 IEEE International Conference on Computational Photography (ICCP). IEEE; 2015. p. 1–10. doi:10.1109/ICCPHOT.2015.7168378. ISBN 978-1-4799-8667-5

[8] Yang F, Wang Z, Wen Y, Qu W. Two-dimensional phase unwrapping algorithms for fringe pattern analysis: a comparison study; 2015. p. 93023F. doi:10.1117/12.2081130. http://proceedings.spiedigitallibrary.org/proceeding.aspx?doi=10.1117/12.2081130

[9] Ghiglia D, Pritt M. Two-dimensional phase unwrapping: theory, algorithms, and software. Wiley; 1998. ISBN 9780471249351, https://books.google.com.mx/books?id=pQtTAAAAMAAJ

[10] Flynn TJ. Two-dimensional phase unwrapping with minimum weighted discontinuity. Journal of the Optical Society of America A 1997;14(10):2692. doi:10.1364/JOSAA.14.002692. https://www.osapublishing.org/abstract.cfm?URI=josaa-14-10-2692

[11] Schofield M, Zhu Y. Fast phase unwrappng algorithm for interferometric applications. Opt Lett 2003;28:1194–6. doi:10.1364/OL.28.001194.

[12] Estrada JC, Servin M, Quiroga JA. Noise robust linear dynamic system for phase unwrapping and smoothing. Optics Express 2011;19(6):5126. doi:10.1364/OE.19.005126. http://www.opticsexpress.org/abstract.cfm?URI=oe-19-6-5126 https://www.osapublishing.org/oe/abstract.cfm?uri=oe-19-6-5126.

[13] de Souza JC, Oliveira ME, dos Santos PAM. Branch-cut algorithm for optical phase unwrapping. Optics Letters 2015;40(15):3456. doi:10.1364/OL.40.003456. https://www.osapublishing.org/abstract.cfm?URI=ol-40-15-3456

[14] Herráez MA, Burton DR, Lalor MJ, Gdeisat MA. Fast two-dimensional phase-unwrapping algorithm based on sorting by reliability following a noncontinuous path. Appl Opt 2002;41(35):7437–44. doi:10.1364/AO.41.007437. http://ao.osa.org/abstract.cfm?URI=ao-41-35-7437

[15] Estrada JC, Vargas J, Flores-Moreno JM, Quiroga JA. Windowed phase unwrapping using a first-order dynamic system following iso-phase contours. Applied Optics 2012;51(31):7549. doi:10.1364/AO.51.007549. https://www.osapublishing.org/abstract.cfm?URI=ao-51-31-7549

[16] Marklund O. Noise-insensitive two-dimensional phase unwrapping method. Journal of the Optical Society of America A 1998;15(1):42. doi:10.1364/JOSAA.15.000042. http://www.opticsinfobase.org/abstract.cfm?URI=JOSAA-15-1-42 https://www.osapublishing.org/abstract.cfm?URI=josaa-15-1-42

[17] Servin M, Cuevas FJ, Malacara D, Marroquin JL, Rodriguez-Vera R. Phase unwrapping through demodulation by use of the regularized phase-tracking technique.. Appl Opt 1999;38(10):1934–41. doi:10.1364/AO.38.001934. http://www.ncbi.nlm.nih.gov/pubmed/18319748 http://ao.osa.org/abstract.cfm?URI=ao-38-10-1934

[18] Rivera M, Marroquin JL. Half-quadratic cost functions for phase unwrapping.. Optics letters 2004;29(5):504–6. http://www.ncbi.nlm.nih.gov/pubmed/15005207

[19] Hocine F, Fekir M, Haddoud A, Belhadj-aissa S, Belhadj-aissa A. A new 2d/3d phase unwrapping strategy of differential interferograms sar. J Indian Soc Remote Sens 2015;43(2):199–212. doi:10.1007/s12524-014-0398-0.

[20] Abdul-Rahman H, Arevalillo-Herráez M, Gdeisat M, Burton D, Lalor M, Lilley F, et al. Robust three-dimensional best-path phase-unwrapping algorithm that avoids singularity loops. Applied Optics 2009;48(23):4582. doi:10.1364/AO.48.004582. https://www.osapublishing.org/abstract.cfm?URI=ao-48-23-4582, 1301.2786

[21] tao Liu W, Tang X, Ma Y, Gao J-H. 3D phase unwrapping using global expected phase as a reference: application to mri global shimming.. Magn Reson Med 2013;70 1:160–8.

[22] Hooper A, Zebker HA. Phase unwrapping in three dimensions with application to insar time series. J Opt Soc Am A 2007;24(9):2737–47. doi:10.1364/JOSAA.24.002737. http://josaa.osa.org/abstract.cfm?URI=josaa-24-9-2737

[23] Itoh K. Analysis of the phase unwrapping algorithm.. Applied optics 1982;21(14):2470. http://www.ncbi.nlm.nih.gov/pubmed/20396058

[24] Imperatore P, Pepe A, Lanari R. Multichannel phase unwrapping: problem topology and dual-level parallel computational model. IEEE Trans Geosci Remote Sens 2015;53(10):5774–93. doi:10.1109/TGRS.2015.2430619.

[25] Serra J. Introduction to mathematical morphology. Computer Vision, Graphics, and Image Processing 1986;35:83–305. doi:10.1016/0734-189X(86)90002-2.

[26] Zhang J, Zhang Y, Wang J, Cai P, Luo C, Qian Z, et al. Characterizing iron deposition in parkinson's disease using susceptibility-weighted imaging: an in vivo mr study. Brain Res 2010;1330:124–30.

[27] Wang Y, Butros SR, Shuai X, Dai Y, Chen C, Liu M, et al. Different iron-deposition patterns of multiple system atrophy with predominant parkinsonism and idiopathetic parkinson diseases demonstrated by phase-corrected susceptibility-weighted imaging. American Journal of Neuroradiology 2012;33(2):266–73.
[28] Liu S, Buch S, Chen Y, Choi H-S, Dai Y, Habib C, et al. Susceptibility-weighted imaging: current status and future directions. NMR Biomed 2017;30(4):e3552.
[29] Ghassaban K, Liu S, Jiang C, Haacke EM. Quantifying iron content in magnetic resonance imaging. Neuroimage 2018.
[30] Pruessmann KP, Weiger M, Scheidegger MB, Boesiger P. Sense: sensitivity encoding for fast mri. Magn Reson Med 1999;42(5):952–62.